

RESEARCH

Open Access



# Investigation of the Deformation and Failure Characteristics of High-Strength Concrete in Dynamic Splitting Tests

Xudong Chen<sup>1\*</sup> , Jin Wu<sup>1</sup>, Kai Shang<sup>1</sup>, Yingjie Ning<sup>2</sup> and Lihui Bai<sup>2</sup>

## Abstract

The dynamic response properties of concrete have been of interest during the use of buildings due to seismic, impact, and explosion events. The splitting Hopkinson lever is a classical device for testing the dynamic mechanical properties of materials. In this paper, dynamic splitting tests on concrete were conducted using it, and a time series predictive computational model for the incident, reflected and transmitted pulses of high-strength concrete specimens at high strain rates was developed, and the extension mechanism of splitting tensile cracks in high-strength concrete was detected and analyzed based on the DIC technique. The results show that: the peak strength of C60 specimens and C80 specimens increased by about 60% and 90%, respectively, from 0.05 MPa to 0.09 MPa in impact strength; the triangular damaged area at the end of the contact surface of the specimen and the rod subjected to high impact pressure increased significantly, the dynamic energy dissipation increased, and the damage degree of the specimens increased; under the action of high strain rate, the brittleness of the concrete specimens with higher strength increased, the damage rate. The higher strength concrete specimens have increased brittleness, faster damage rate and higher crack extension under high strain rate. The results of the paper can provide important references for the design of buildings under impact loading.

**Keywords:** high-strength concrete, separated Hopkinson compression bars, dynamic splitting test, nonlinear regression analysis, digital image correlation

## 1 Introduction

Concrete is widely used in civil engineering and military facilities, and the analysis of the mechanical properties of concrete under static or quasi-static loading has been the subject of extensive research by scholars worldwide in recent decades. A more mature theoretical system has been formed in the study of the static mechanics of concrete structures, and the force characteristics and deformation features of concrete in general under static loading are understood. During their service life, they

may be subjected to impact loads, such as explosions and shocks (Li et al., 2004). It is very important to study the dynamic properties of concrete materials. However, due to the complexity and variability of the factors affecting the dynamic mechanical properties of concrete (Su et al., 2016; Wu et al., 2015), and due to the late start of research on the dynamic mechanical properties of concrete and the limitations of research methods, the study of the dynamic mechanical properties of concrete, especially for high-strength concrete, is still a great challenge for many scholars.

Under the action of blast load and impact load, the tensile effect caused by the stress pulse reflected from the edge of the specimen has a significant impact on the failure of the specimen (Li et al., 2020; Chen et al., 2021; Jiang et al., 2020). Therefore, the dynamic splitting

Journal information: ISSN 1976-0485 / eISSN2234-1315.

\*Correspondence: cxdong1985@hotmail.com

<sup>1</sup> College of Civil and Transportation Engineering, Hohai University, Nanjing 210098, China

Full list of author information is available at the end of the article



© The Author(s) 2022. **Open Access** This article is licensed under a Creative Commons Attribution 4.0 International License, which permits use, sharing, adaptation, distribution and reproduction in any medium or format, as long as you give appropriate credit to the original author(s) and the source, provide a link to the Creative Commons licence, and indicate if changes were made. The images or other third party material in this article are included in the article's Creative Commons licence, unless indicated otherwise in a credit line to the material. If material is not included in the article's Creative Commons licence and your intended use is not permitted by statutory regulation or exceeds the permitted use, you will need to obtain permission directly from the copyright holder. To view a copy of this licence, visit <http://creativecommons.org/licenses/by/4.0/>.

test properties of concrete play an important role in the safety of concrete structures (Paiak et al., 2021). A separate Hopkinson pressure bar (SHPB) test can perform dynamic mechanical properties of concrete under high-speed impact and can eliminate the effect of axial inertia in the test (Bertholf et al., 1975; Gong et al., 2019). Yang et al. (2015) conducted a Brazilian disc test on mortar using a separate Hopkinson pressure bar (SHPB) device and found that mortar is a strain rate sensitive material. Khan et al. (2019) simulated the actual stress state of concrete structures under dynamic loads, such as earthquakes, and dynamic splitting tests under variable lateral pressure were conducted to investigate the connection between the measured pressure and strain rate and the splitting test strength of concrete. It was found that the increase in strain rate could increase the strength and splitting modulus of concrete splitting test strength (Huang et al., 2022), which is consistent with the results of Chen's study (Chen et al., 2017). It is known that materials behave differently under static and dynamic loads (Miao, 2018; Renliang et al., 2019; Zwiessler et al., 2017). In dynamic loading, the frictional and inertial forces at the concrete ends produce additional constraints in the concrete, resulting in lateral forces and multi-axial stress states in the concrete (Pająk et al., 2019). In SHPB tests, the frictional forces at the ends can be minimized by applying petroleum jelly and polyester foil to the specimen surface (Durand et al., 2016).

For concrete, the displacement and strain can be analyzed using DIC after the mechanical properties test (Shah et al., 2011; Skarżyński et al., 2018). Concrete is a material commonly used in the construction industry and knowing its displacement and strain helps to determine the pattern of cracks on the concrete surface and many other properties, so it is important to perform such tests and analyses on concrete. Hamrat et al. (2016) used the digital image correlation (DIC) technique for ordinary concrete and high-strength concrete for flexural performance experimental study of their crack width and strain measurements, it was found that the DIC technique can measure and track the crack width variation with high accuracy. Liu et al. (2019) used the DIC technique for capturing the detailed formation and expansion of cracks during loading. The strain data obtained from the DIC method was compared and validated with the strain data obtained from the conventional method (strain gauges). DIC has proven to be a reliable and accurate non-contact testing method that can be successfully used to determine the mechanical properties of various concrete materials (Huang et al., 2019; Mróz et al., 2020). However, at the present stage, DIC technology is mainly applied to the measurement of quasi-static deformation of materials, and the research related to dynamic tests

is less. The application of DIC technology to dynamic tests, combined with high-speed cameras to achieve high frame rate filming conditions, can effectively solve the difficulty of fine measurement of deformation under impact loading of materials.

In this study, the dynamic splitting tensile properties of high-strength concrete (C60 and C80) at different impact strength was investigated using SHPB tests, and the changes in damage morphology, dynamic splitting tensile strength, and dynamic dissipation energy with impact strength and strain rate were analyzed. By predicting the distribution characteristics of the strain waveform of high-strength concrete under a high strain rate with time, the corresponding computational model was established. In addition, the crack extension mechanism of high-strength concrete was detected and analyzed by the digital image correlation (DIC) technique, and the crack extension and strain variation of high-strength concrete in splitting and tensile tests were determined with high accuracy. The purpose of this study is to investigate the splitting and tensile processes and damage mechanisms of high-strength concrete under different impact strengths and to propose strain-related scaling laws and damage modes for brittle materials under dynamic splitting and tensile conditions.

## 2 Materials and Methods

### 2.1 Materials and Specimen Preparation

The raw materials used in this test include P-II 52.5 silicate cement, Class F Grade I fly ash, slag powder, silica fume, and nakasand with fineness modulus of 2.6, 5–20 mm crushed stone, and high-performance water reducing agent with 30% water reduction rate. The physicochemical properties of the cement are shown in Table 1. To maintain the same size of the specimens used in the dynamic test, specimens with an aspect ratio of 0.5 are usually used (Dai et al., 2010). Therefore, the specimens used in this test for the dynamic splitting are  $\phi$  100 mm  $\times$  50 mm cylindrical specimens. The ratio design of C60 and C80 high-strength concrete prepared for this test is shown in Table 2.

### 2.2 Test Methods

#### 2.2.1 Static Mechanical Properties

According to the requirements of GB T50081-2002 (2002), 100 mm  $\times$  100 mm  $\times$  300 mm prismatic specimens and  $\phi$  100 mm  $\times$  200 mm cylindrical specimens were used for the elastic modulus test and static mechanical property test, respectively.

Five specimens of C60 and C80 strengths were taken and the average value was obtained to obtain the modulus of elasticity of the high-strength concrete specimens.

**Table 1** Physicochemical properties of cement.

Materials	Quality fraction (%)					Condensation time			Specific surface area (m <sup>2</sup> /kg)	
	CaO	SiO <sub>2</sub>	Fe <sub>2</sub> O <sub>3</sub>	Al <sub>2</sub> O <sub>3</sub>	MgO	K <sub>2</sub> O	SO <sub>3</sub>	Initial condensation (min)		Final condensation (min)
Cement	70.40	17.17	4.15	3.75	1.69	0.95	0.83	110	215	326.7

**Table 2** Design of high-strength concrete ratio (m<sup>3</sup>/kg).

Types	Nakasand	Stone	Cement	Slag powder	Fly ash	Silica fume	Water	High-performance water reducing agent
C60	677	1004	234	94	141	–	150	5.6
C80	647	1056	462	84	–	54	135	18

**Table 3** Basic mechanical property parameters of high-strength concrete.

Types	Compressive strength (MPa)	Tensile strength (MPa)	Elastic modulus (GPa)
C60	70.1	5.4	40.8
C80	84.3	6.8	43.1

The elastic modulus can be calculated by the following formula:

$$E = \frac{\sigma_{1/3} - \sigma_{0.5}}{\varepsilon_{1/3} - \varepsilon_{0.5}}, \quad (1)$$

where  $E$  is the Elastic modulus;  $\sigma_{1/3}$  is 1/3 of the axial compressive strength of the prismatic specimen;  $\sigma_{0.5} = 0.5$  MPa;  $\varepsilon_{1/3}$  and  $\varepsilon_{0.5}$  are the strains corresponding to  $\sigma_{1/3}$  and  $\sigma_{0.5}$ , respectively, during loading.

According to the relevant test requirements of GB T50081-2002 (2002), this paper conducted elastic modulus tests and static mechanical property tests on two kinds of high-strength concrete specimens, and the basic mechanical property parameters of high-strength concrete were measured, as shown in Table 3.

### 2.2.2 Dynamic Splitting Test

Usually, a key factor affecting the deformation behavior under dynamic loading is the impact pressure (Chen et al., 2020; Huang et al., 2020). For many materials, the mechanical behavior under different impact pressures may vary significantly (Frew et al., 2005). Mechanical properties based on static tests can be misleading and may significantly underestimate or overestimate the effective properties under dynamic impact conditions (Huang et al., 2020). In dynamic impact testing, the split Hopkinson pressure bar (SHPB) is an effective method for testing the dynamic properties of materials (Li et al., 2000).

The SHPB test is based on two basic assumptions. One is the assumption of a one-dimensional stress wave of the elastic rod, that is, the pressure rod is always in the elastic strain range during the experiment (this assumption can be satisfied if the stiffness of the rod is much greater than the stiffness of the specimen); the second is

that the stress and strain in the specimen are uniformly distributed along the axial direction of the specimen, that is, the assumption of uniformity (this assumption can be satisfied if the length of the specimen is much smaller than the wavelength of the stress wave). These two basic assumptions are satisfied to obtain valid experimental results (Gong et al., 2019).

In this test, the dynamic splitting test properties of high-strength concrete (C60 and C80) specimens were tested using a 100-mm-diameter split Hopkinson pressure bar (SHPB) as a dynamic loading device. As shown in Fig. 1, the SHPB mainly consists of a driving system, an incident bar, a transmission bar, an absorber bar, and a data acquisition system. The lengths of the incidence rod and transmission rod are 4 m and 3 m, respectively. The bullet, incidence rod, transmission rod, and absorption rod in the compression rod system are composed of high-strength 40Cr alloy steel with a density of 7800 kg/m<sup>3</sup>, an elastic modulus of 250 GPa, and a yield strength of 800 MPa.

During the test, the specimen needs to be clamped between the incident and transmission rods so that the two opposite surfaces of the specimen are parallel to the axis of the compression rod and the midpoint of the contact line between the specimen and the rod coincides with the center point of the end of the rod. A thin layer of lubricant is applied to the interface between the specimen and the rod contact to minimize the effect of frictional effects. The impact pressures set for this test are 0.05 MPa, 0.06 MPa, 0.07 MPa, 0.08 MPa, and 0.09 MPa (Table 4). Under the impact of the air pump pressure, the bullet strikes the incident rod and an incident wave is formed. This incident wave propagates between the incident rod and the specimen, forming a transmission wave and a reflection wave, which enter the transmission rod and the reflection rod, respectively.

The incident and reflected waves are collected by a strain gauge attached to the incident rod, and the transmitted waves are collected by a strain gauge attached to the transmission rod. Under each impact pressure, five specimens were tested for each of the two specimens, and the average of the dynamic splitting test strength of the specimens was calculated to be the dynamic splitting test strength. The response of the concrete specimens

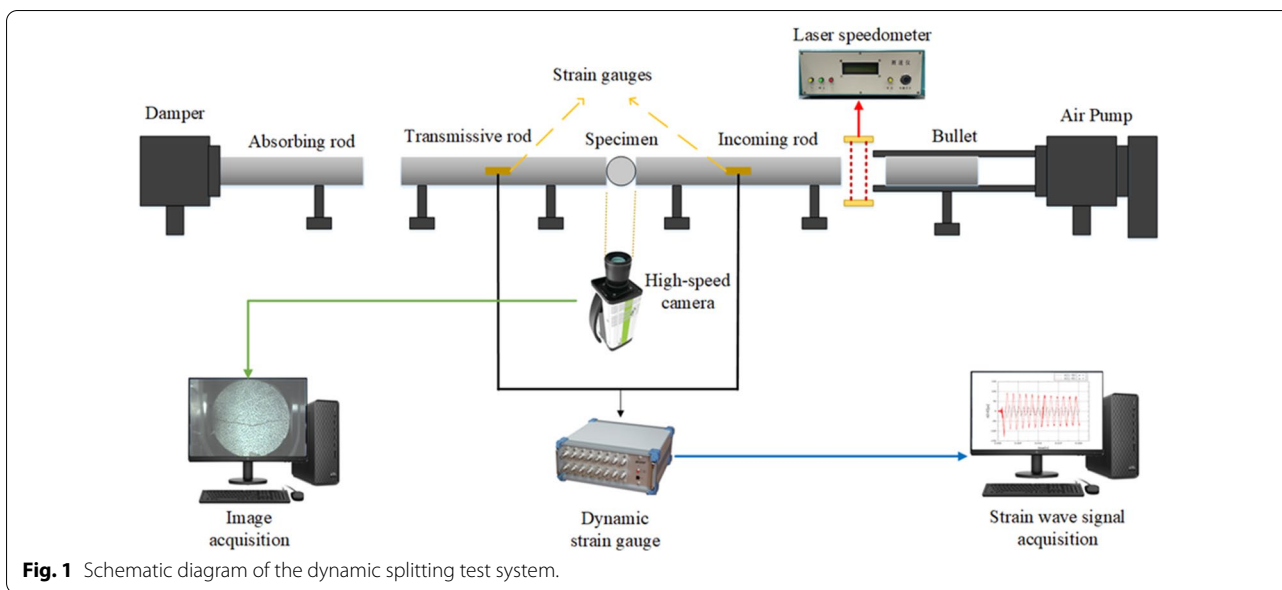


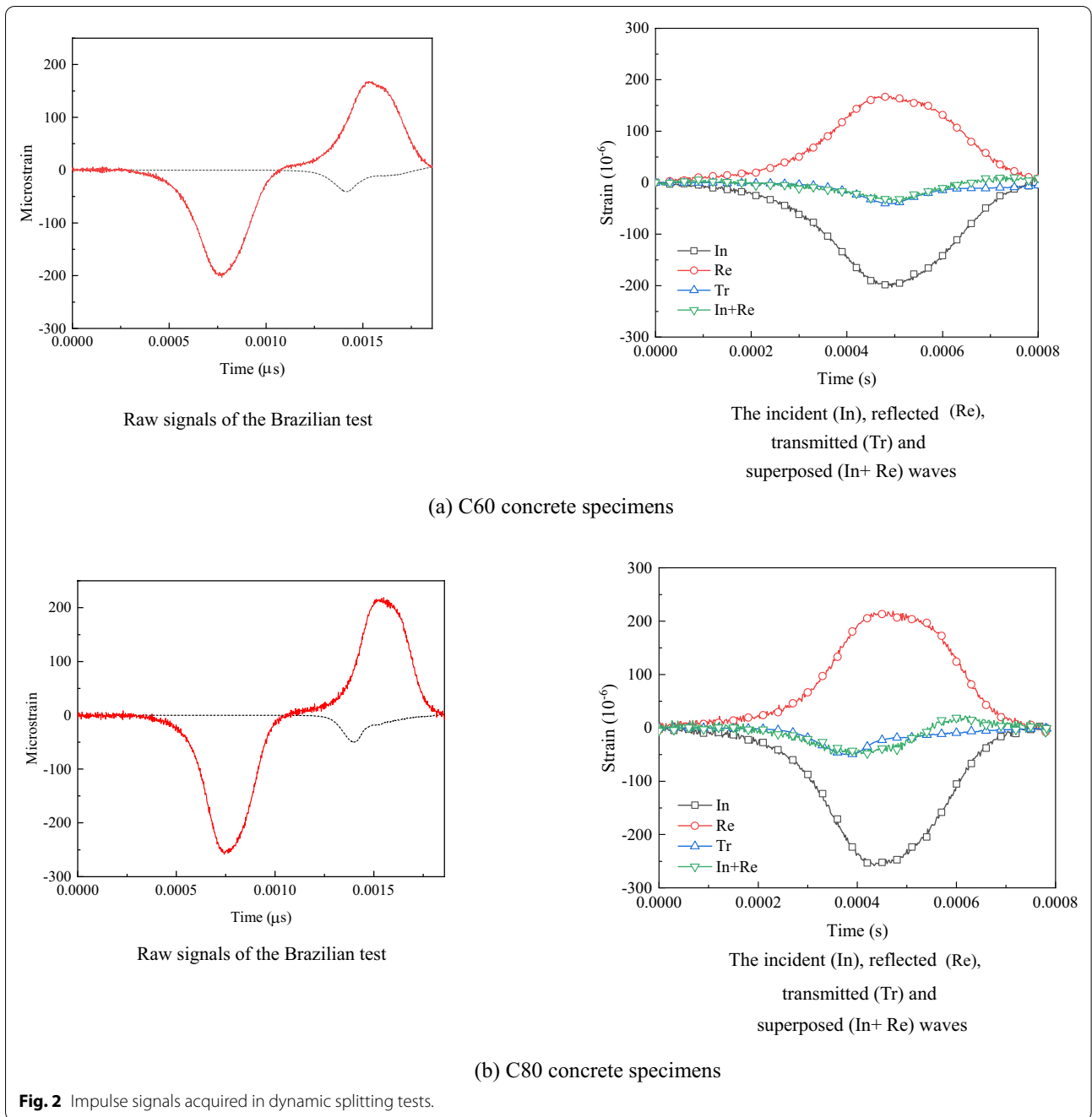
**Table 4** SHPB dynamic splitting and pulling tests.

Types	Impact strength (MPa)
C60	0.05
	0.06
	0.07
	0.08
	0.09
C80	0.05
	0.06
	0.07
	0.08
	0.09

measured by the SHPB system under impact loading is shown in Fig. 2. The figures "Raw signals of the Brazilian test" show typical impulse signal curves recorded by strain gauges on the incident and reflected bars as incident, reflected, and transmitted waves, respectively. It should be noted that the reflected signals are very weak compared to the incident or reflected waves. This is mainly because the splitting tensile strength of the concrete is lower than the compressive strength. Therefore, after the damage of the specimen, most of the elastic stress waves are reflected as tensile waves from the incident rod. The figures "The incident (*In*), reflected (*Re*), transmitted (*Tr*) and superposed (*In+Re*) waves" show the stress balance check in the case of eliminating the

time difference between the three waves, which is the result of the dynamic loading process. This is an important indicator of the validity of the data on whether the specimen achieves stress equilibrium in the dynamic loading process. According to the three-wave equilibrium theory, the specimen is considered to be in stress equilibrium when the incident and reflected stresses are equal to the transmitted stress. In addition, the shaping sheet technology was used during the test to extend the stress wave rise time and further achieve the stress equilibrium state by achieving multiple reflections of the stress wave in the specimen.

As shown in Fig. 2, the typical pulse of some high-strength concrete specimens under dynamic impact strength are shown. It can be seen that the transmitted wave (*Tr*) is much smaller than the incident wave (*In*) and the reflected wave (*Re*), and the transmitted wave (*Tr*) always remains the same as the sum of the incident wave and the reflected wave (*In+Re*) during the whole loading process. In addition, the incident wave (*In*) and reflected wave (*Re*) is much larger for C80 concrete specimens, which is due to the higher dynamic splitting test strength of C80 concrete than that of C60 concrete. The rate of increase of the incident pulse slows down with the plastic deformation of the pulse shaper after the bullet rushes out of the impact and causes the incident, reflected, and transmitted pulses to reach their peaks almost simultaneously (Chen et al., 2015). It is important to note that the transmitted wave is very weak compared to the incident or reflected wave. This is mainly because the splitting tensile strength of concrete are lower than



its compressive strength. Therefore, after the specimen is damaged, most of the stress waves are reflected as tensile waves along the incident rod.

According to the stress wave theory (Khosravani et al., 2018; Chen et al., 2018), the dynamic splitting test load, dynamic splitting test strength, and strain rate of high-strength concrete can be calculated using the following equations:

$$\begin{cases} P_{dsr}(t) = E_b A_b \varepsilon_t(t) \\ \sigma_{dst}(t) = \frac{2P_{dst}(t)}{\pi ld} = \frac{2E_b A_b \varepsilon_t(t)}{\pi ld} \\ \dot{\varepsilon} = \frac{\sigma_{dst}}{\Delta t E} \end{cases}, \quad (2)$$

where  $P_{dsr}(t)$  is the dynamic splitting test load of the high-strength concrete specimen over time.  $E_b$  and  $A_b$  are the elastic modulus and cross-sectional area of the separated Hopkinson compression bar, respectively.  $\varepsilon_t(t)$  is the transmitted strain signal.  $\sigma_{dst}(t)$  is the dynamic

splitting test stress of the specimen over time.  $l$  and  $d$  are the length and diameter of the specimen, respectively.  $\dot{\epsilon}$  is the dynamic splitting test strain rate of the specimen.  $\Delta t$  is the time required to reach the peak dynamic load, and  $E$  is the static modulus of elasticity of the high-strength concrete specimen.

### 2.2.3 Digital Image Correlation Technique

The digital image correlation (DIC) technique is a photomechanical technique that calculates selected target surface displacements in a series of digital images with high accuracy (Pan et al., 2018). The images are recorded during the test and then post-processed. In recent years, the rapid development of high-speed digital cameras has made possible full-field deformation-related measurements in SHPB tests, which, when combined with surface structure tracking methods, such as DIC, can provide at least tens of high-resolution images at high frame rates (Sharafisafa et al., 2020). The first image is called the "reference image" and the second image is called the "deformation image". Usually, the DIC first defines a grid of analysis points on the reference image. In order for the method to identify the deformation points, a speckle image is usually created by hand. Black paint is sprayed on the white surface of the specimen at a distance of about 50 cm from the sprayer, which is long enough to spray small black spots on the specimen while avoiding producing too many black spots that would cover the entire surface. To obtain effective correlation, the scatter pattern should be non-repetitive, isotropic, and high contrast, i.e., a random pattern that does not show a tendency toward a certain direction and shows dark blacks and bright whites of sufficient size for high strain resolution. By creating this type of pattern, a very sensitive bokeh is avoided. Then, a set of pixels often called "subsets", is defined at each node of the grid. Image correlation is performed for each node by identifying the most similar subsets of the deformed image based on some statistical calculations of image correlation within each subset (Sharafisafa et al., 2020; Braunagel et al., 2020; Gao et al., 2020).

In this test, to ensure accurate measurement of DIC, artificial textures were added to the lightly painted surface of the test piece to improve the collected data results (Fig. 3). In addition, the two-dimensional DIC method used in this test allows monitoring and evaluating the displacement changes along the shear surface of the specimen with the strain changes caused by curvature. Based on this feature, images of the splitting test damage process of high-strength concrete specimens during the SHPB test were collected in this study, and the specimen crack width and strain data were obtained based on the

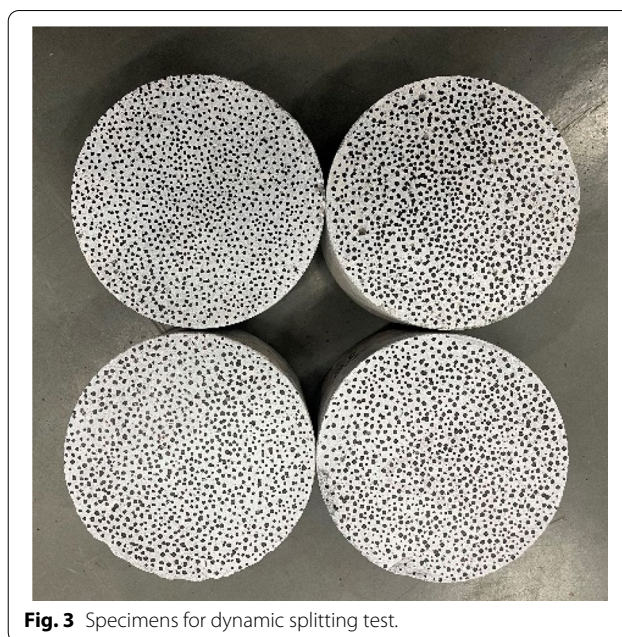


**Fig. 3** Specimens for dynamic splitting test.

processing and analysis of the DIC technique for monitoring the deformation of the structure.

## 3 Test Results and Analysis

### 3.1 Analysis of Damage Patterns

Figs. 4 and 5 show the damage morphology of the specimens of C60 and C80 high-strength concrete specimens under different impact strengths (0.05 MPa, 0.06 MPa, 0.07 MPa, 0.08 MPa, 0.09 MPa), respectively. Comparing the damage morphology of high-strength concrete under different impact conditions, it can be seen that under lower impact pressures, the specimens were crushed into large fragments, and with the increase of impact strength, the damage degree of edge damage of the specimens increased, and the crack width increased. In addition, with the increase of impact strength, the size of the fragments under the specimen crushed and spalled became smaller, and the damage mode gradually changed from longitudinal splitting damage to crushing damage.

The crack extensions of C60 and C80 concrete at different impact pressures are shown in Fig. 6, as observed using a high-speed camera. According to the principle of the dynamic Brazilian disc splitting test, the splitting tensile stress at the center of the specimen is maximum when the specimen is subjected to the impact load (Khan et al., 2019). Therefore, as shown in Fig. 6, under the impact pressure, the splitting crack first developed at the center of the specimen and gradually extended straight along the radial direction, where the load was applied, eventually splitting the specimen into two halves. Comparing

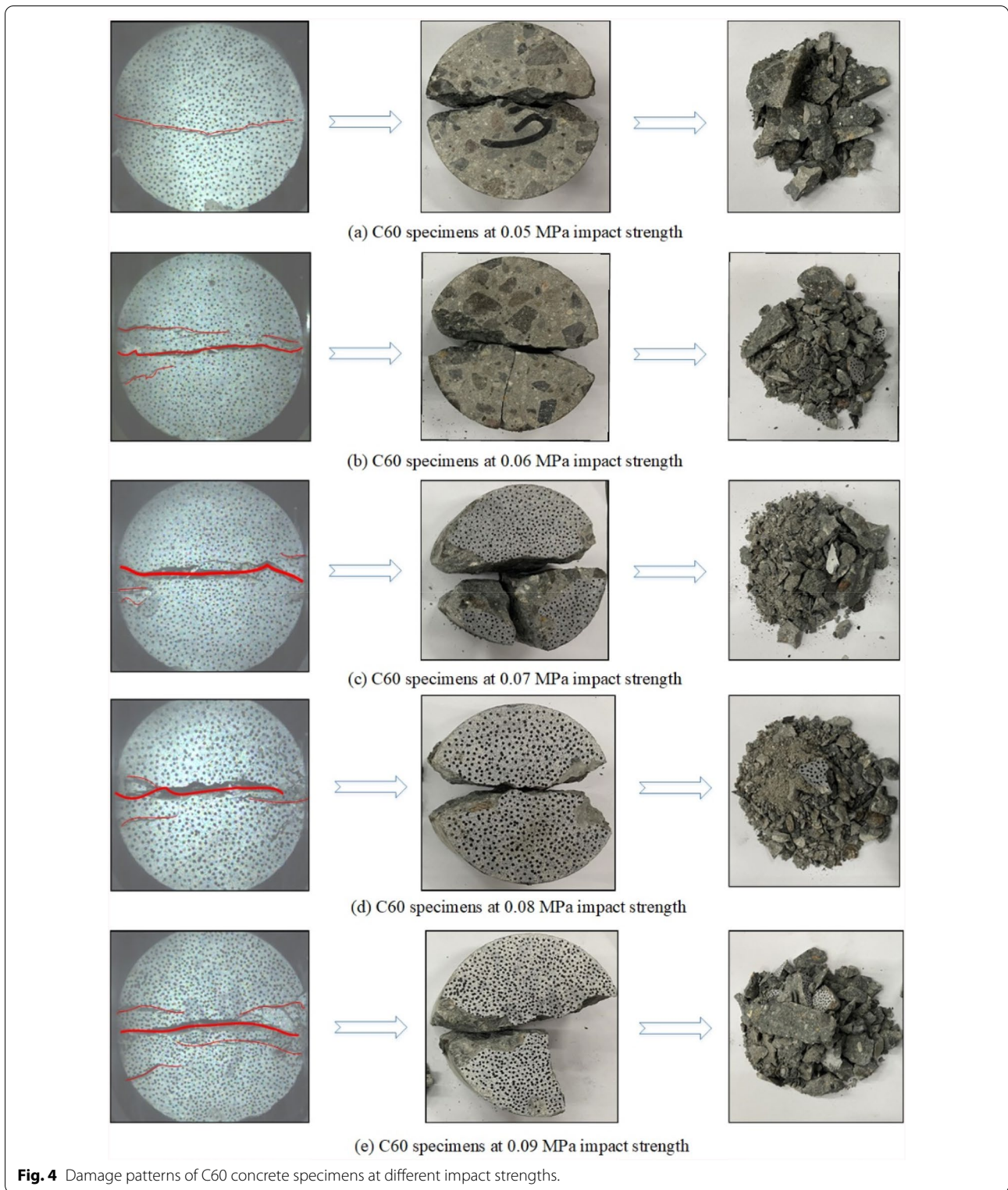
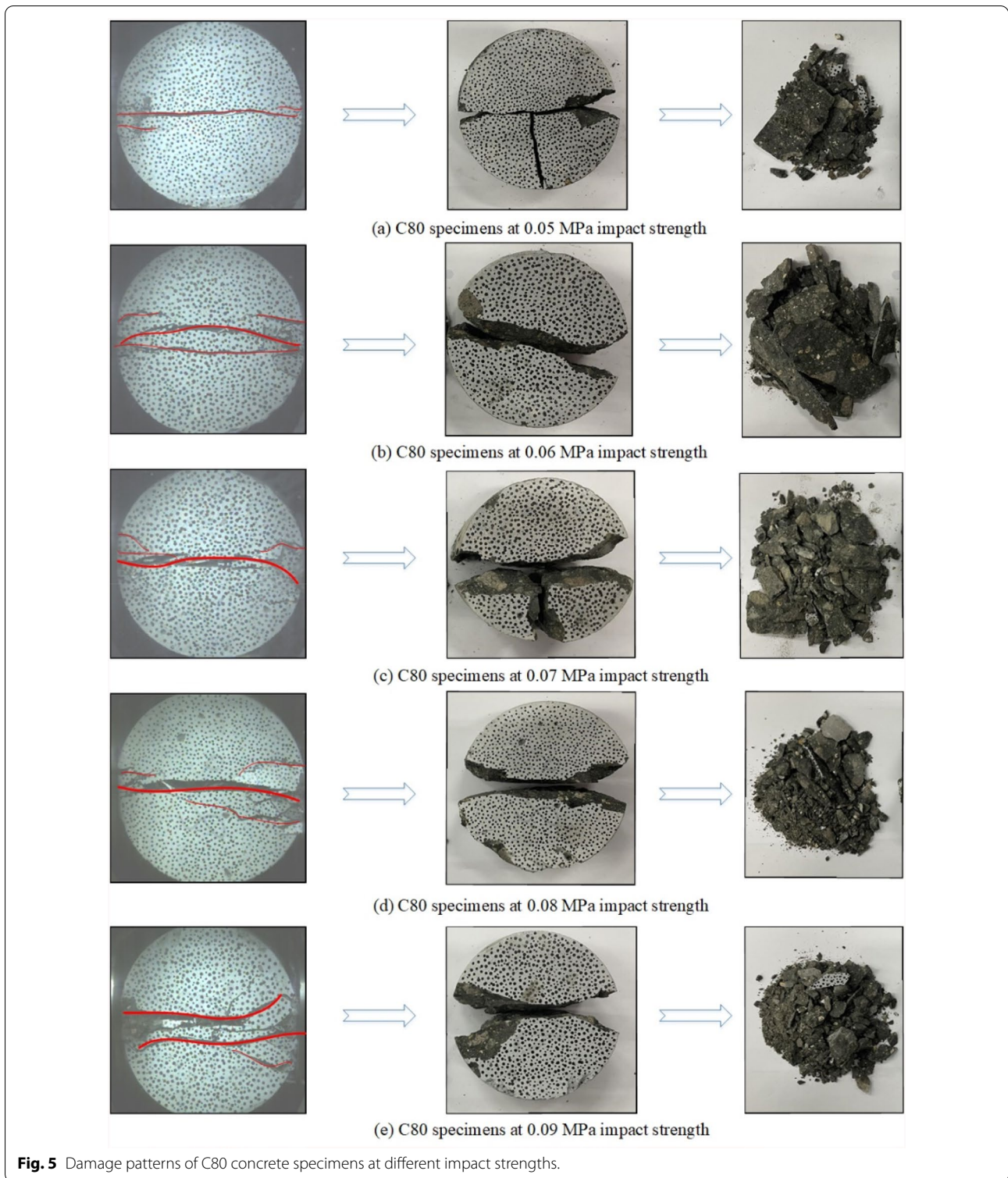


Fig. 6a, b and c, d, it is easy to see that when the impact pressure was small, the cracks of the specimen are relatively flat and extended along a single path with relatively

small crack width. When the impact pressure increased, the specimens showed secondary cracks with curved crack expansion paths and increased dynamic energy



dissipation. Compared with the low impact pressure, the triangular damaged area at the end of the contact surface of the specimen and the rod subjected to high impact pressure increased significantly, some secondary

fragments were formed, and the damage to the specimen increased. It is noteworthy that the primary cracking starts from the center and expands towards both ends. As time increases, the high strain region becomes larger and

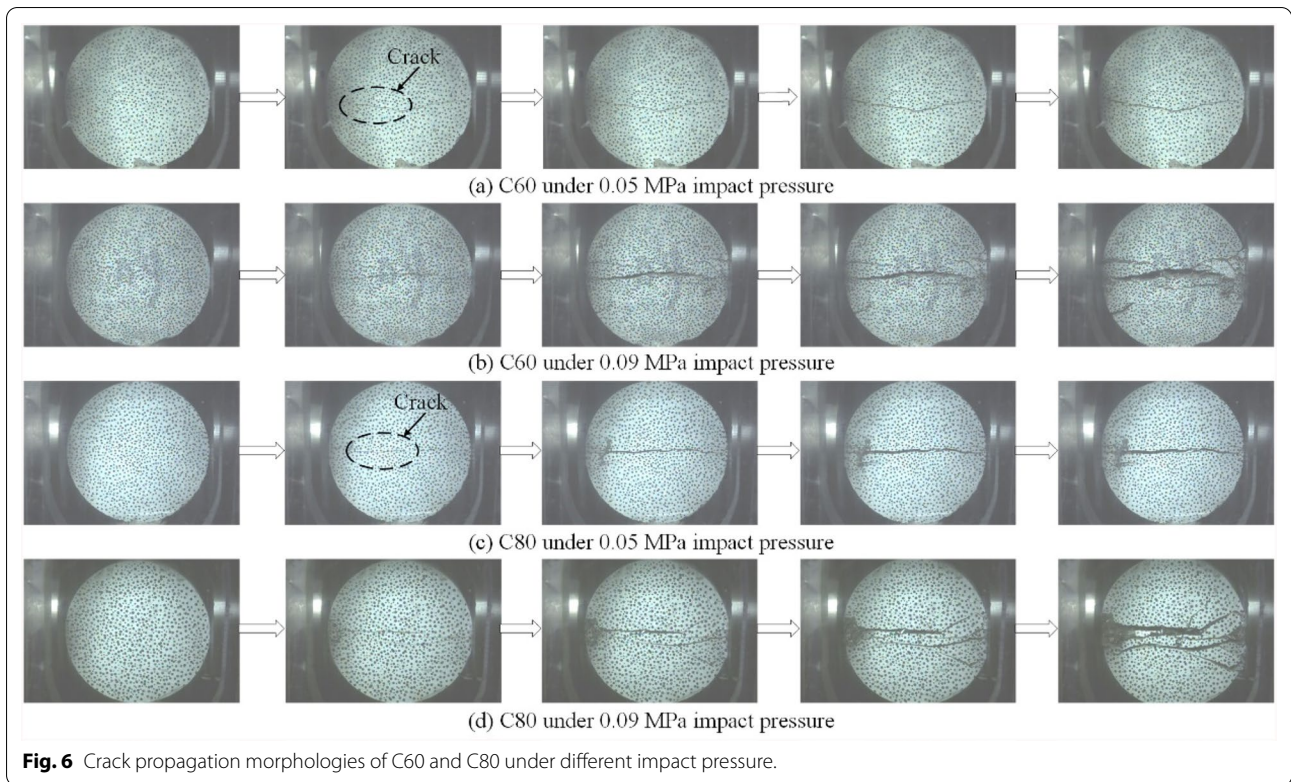


**Fig. 6** Crack propagation morphologies of C60 and C80 under different impact pressure.

expands and there is a secondary strain concentration region at the end. In this process, the cracking and the strain concentration region are initiated and expanded simultaneously. At higher impact loads, it can be seen that the stress concentration pattern deviates from the horizontal direction as the loading process proceeds.

### 3.2 Dynamic Splitting Test Stress–Strain Response

Fig. 7a, b shows the dynamic splitting test stress–strain response of C60 concrete and C80 concrete, respectively. After the air pump in the detached Hopkinson, compression rod device is pressurized to the specified impact strength value, the bullet is shot and then splits

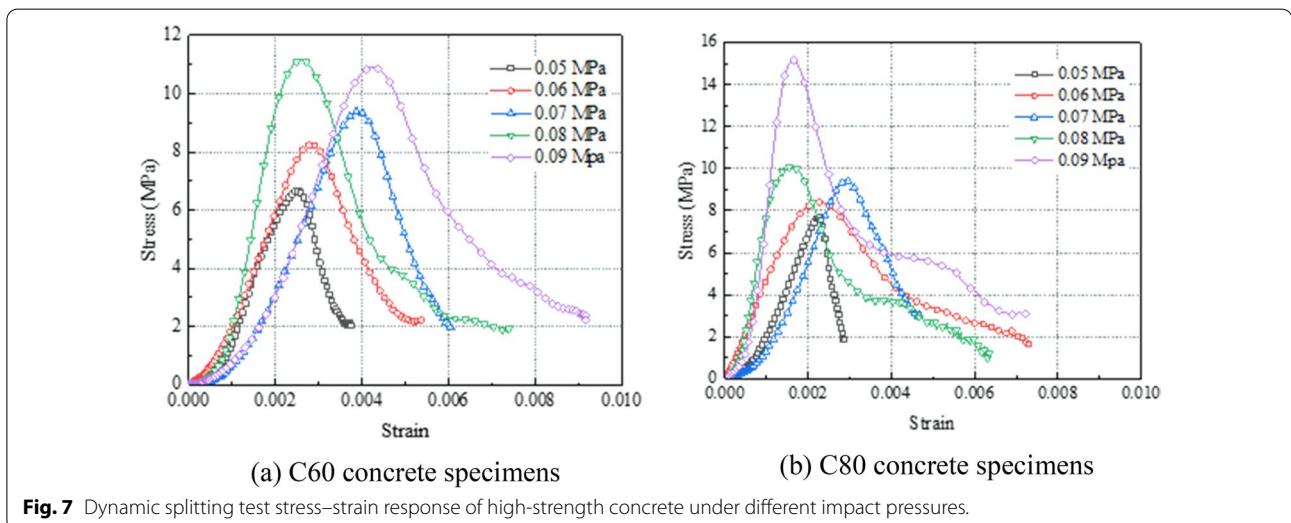


**Fig. 7** Dynamic splitting test stress–strain response of high-strength concrete under different impact pressures.

the specimen. As shown in Fig. 7, the dynamic splitting test strength of the high-strength concrete gradually increased with increasing impact pressure. The peak strengths of C60 and C80 specimens increased by about 60% and 90%, respectively, from 0.05 MPa to 0.09 MPa. Moreover, the dynamic splitting test strength of the specimens showed an overall trend of gradual increase in strain corresponding to the final damage. The stress–strain curve of high-strength concrete is similar to that of ordinary concrete, with an initial approximate linear elastic phase, followed by a nonlinear phase increase in stress. After the stress reaches its peak, it then softens. In the softening phase, the stress decrease is smaller for high impact strength.

Ai et al. (2019) found that maintaining a certain impact strength for the bullet to be ejected allows the strain rate at the time of the test to remain within a more stable value, i.e., a determined value of impact strength implies an exact value of strain rate corresponding to it. Dynamic mechanical properties of materials. In the DIF–strain rate relationship plot for the high-strength concrete (C60 and C80) specimens in Fig. 8, the DIF vs. strain rate relationship for C60 concrete is more nearly linear. However, for C80 concrete, a sharp shift in DIF values can be observed as the strain rate increases. the tensile strength of C80 concrete increased slowly at low strain rates, and the strain rate sensitivity of concrete increased significantly when the strain rate exceeded the transition strain rate by about  $27 \text{ s}^{-1}$ . In addition to this, the slope of the fitted line for C60 is 3.59%, and the slope of the fitted line for C80 shifts to 14.84% after taking the lead at 1.42%. This indicates that the sensitivity of C80 to the strain rate effect (Ross et al., 1995) is lower than that of C60 at first

and increases with the increase of strain rate, C80’s sensitivity increases and exceeds that of C60. Combined with the analysis in Fig. 7b, it was found that the peak strength of C80 concrete specimens at an impact strength of 0.9 MPa (high strain rate at this point) had a significant increase, compared to that at an impact strength of 0.5 MPa, the peak strength increases by about 90%. Such a trend corresponds to the DIF–strain rate variation relationship for the C80 specimens in Fig. 8.

### 3.3 Dynamic Dissipation Energy

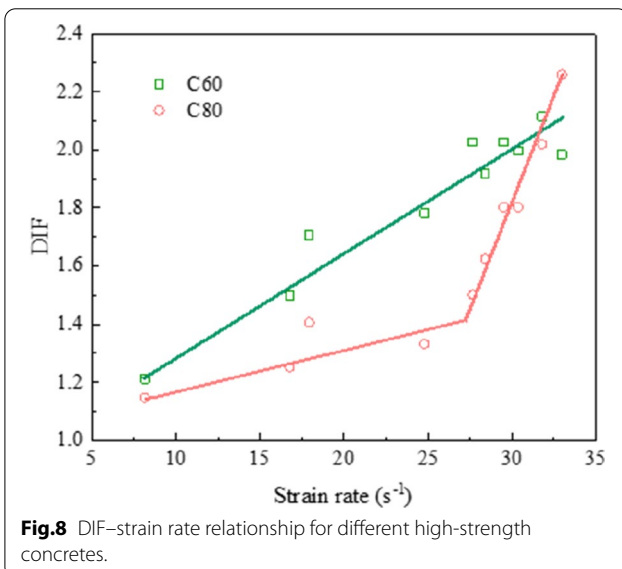
Based on the law of conservation of energy, the energy consumed by high-strength concrete specimens subjected to an impact load can be calculated from the energy carried by the incident, reflected, and transmitted pulses as follows (Feng et al., 2018):

$$W_d = W_i - W_r - W_t, \tag{3a}$$

$$\begin{cases} W_i = E_b A_b C_b \int_0^t \varepsilon_i^2 dt \\ W_r = E_b A_b C_b \int_0^t \varepsilon_r^2 dt \\ W_t = E_b A_b C_b \int_0^t \varepsilon_t^2 dt \end{cases}, \tag{3b}$$

where  $W_d$  is the dissipation energy;  $W_i$ ,  $W_r$ , and  $W_t$  are the energy carried by the incident pulse, reflected pulse, and transmitted pulse, respectively;  $E_b$ ,  $A_b$ , and  $C_b$  are the Elastic modulus, cross-sectional area, and the velocity of the P-wave of the compression bar, respectively;  $\varepsilon_i$ ,  $\varepsilon_r$ , and  $\varepsilon_t$  are the incident strain signal, reflected strain signal, and transmitted strain signal, respectively.

The dynamic dissipation energy of high-strength concrete determined using Eqs. 3(a) and (b) shown in Fig. 9. From Fig. 3, it is easy to find that the dissipation energy of high-strength concrete increases with the increase in impact strength. Under high strain rates, the dissipation energy of C60 specimens is slightly higher than that of C80 concrete specimens. In particular, at an impact strength of 0.09 MPa, when the strain rate is about  $32 \text{ s}^{-1}$ , the dissipation energy at this time is at least 300% higher than the dissipation energy at an impact strength of 0.05 MPa. This is due to the greater brittleness of the concrete material and the greater degree of damage to the specimens at high strain rates. As the impact strength increases, the impact energy also increases, and the dissipation energy of the high-strength concrete specimens increases with the increase in impact energy. In addition to this, as the strain increases, the microcracks generated inside the high-strength concrete specimens increase and the degree of damage to the concrete gradually increases. Fu et al. (2021) found that the energy consumed for the formation of new cracks in concrete is significantly greater than that consumed for the expansion of existing cracks. Therefore, the conclusion obtained from



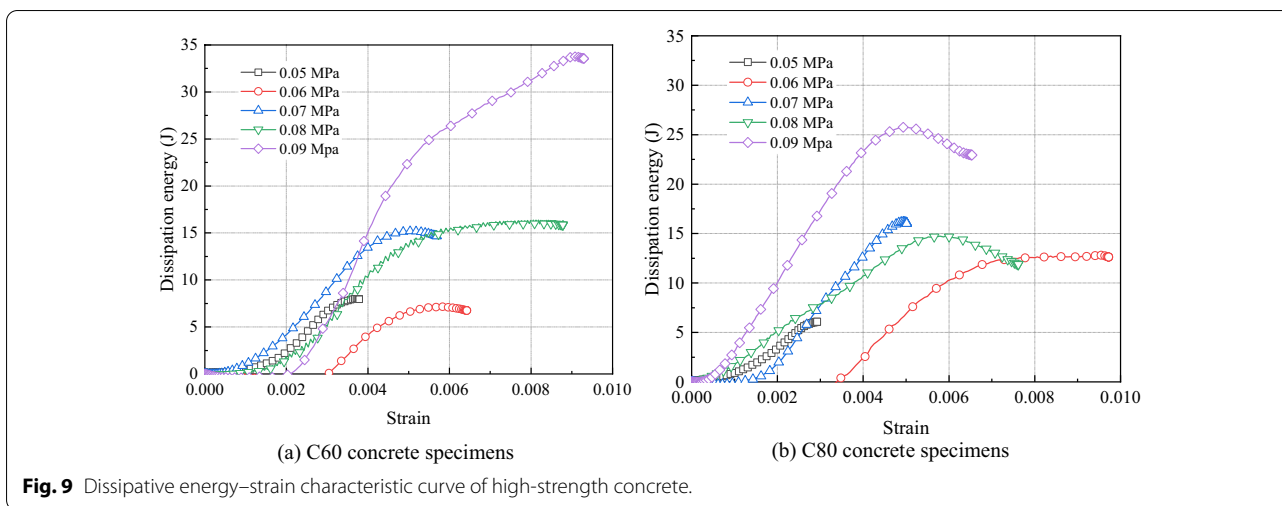


**Fig. 9** Dissipative energy–strain characteristic curve of high-strength concrete.

this test can also corroborate the phenomenon that the energy consumed by high-strength concrete specimens increases with the increase of strain.

### 3.4 Regression Analysis of Impulse Wave Response of Each Rod

In this test, time series equations were developed based on the incident and reflected pulses acquired in the SHPB test, based on a one-dimensional nonlinear regression analysis with the pulse acquisition time  $t$  as the starting point. The incident strain signal and reflected strain signal of high-strength concrete at a high strain rate (impact strength of 0.09 MPa) were predicted, and the confidence interval  $R^2$  was used to evaluate the goodness of the model fit to the sample data.

After Matlab programming and comparing the results of the preliminary runs several times, the equation relationship between the strain signal value and time for this test was initially determined to be a unitary seventh order equation with a confidence interval  $R^2 \geq 0.95$ , with the following equation:

$$\varepsilon = at^7 + bt^6 + ct^5 + k, \tag{4}$$

where  $a, b, c, k$  are model variable coefficients, and the unit of time  $t$  is  $\mu s$ .

After one-dimensional nonlinear analysis by Matlab software, the model coefficients of the nonlinear

**Table 5** Calculated coefficients of C60 and C80 one-dimensional nonlinear regression.

Types	Model variable coefficients				
	$a$	$b$	$c$	$k$	
C60	Incident	$1.94 \times 10^{-15}$	$-4.52 \times 10^{-12}$	$3.93 \times 10^{-9}$	-1.96
	Reflection	$-1.59 \times 10^{-15}$	$3.74 \times 10^{-12}$	$-3.28 \times 10^{-9}$	15.32
C80	Incident	$1.86 \times 10^{-15}$	$-4.52 \times 10^{-12}$	$4.13 \times 10^{-9}$	-6.32
	Reflection	$-1.17 \times 10^{-15}$	$-1.59 \times 10^{-15}$	$-2.85 \times 10^{-9}$	2.94

regression equations of strain signals vs. time for C60 concrete specimens and C80 concrete specimens are shown in Table 5.

Comparing the coefficients of the nonlinear regression equation for C60 and C80 concrete specimens in Table 5, it can be found that the absolute values of the coefficients corresponding to the reflected pulses in the regression coefficient equation for C60 are basically larger than those for C80. This indicates that among the strain values predicted by this nonlinear regression equation for C60 and C80, the reflected strain signal of C60 has a higher correlation with the change in time, i.e., the reflected strain signal of C60 The rate of change with time is faster for C60. Based on the coefficients obtained from the programming calculations, the regression analysis equation for each strength concrete is obtained by substituting them into the univariate nonlinear regression equation as

$$C60 : \begin{cases} \varepsilon_i = 1.94 \times 10^{-15}t^7 - 4.52 \times 10^{-12}t^6 + 3.93 \times 10^{-9}t^5 - 1.96 \\ \varepsilon_r = -1.59 \times 10^{-15}t^7 + 3.74 \times 10^{-12}t^6 - 3.28 \times 10^{-9}t^5 + 15.32, \\ \varepsilon_t = \varepsilon_i + \varepsilon_r \end{cases} \tag{5a}$$

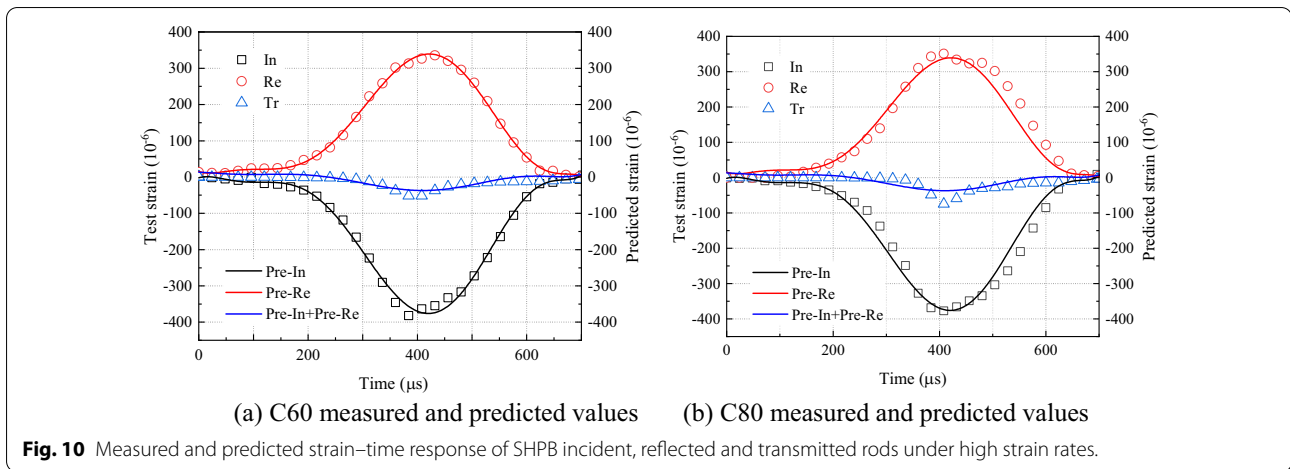


**Fig. 10** Measured and predicted strain–time response of SHPB incident, reflected and transmitted rods under high strain rates.

$$\text{C80} : \begin{cases} \varepsilon_i = 1.86 \times 10^{-15}t^7 - 4.52 \times 10^{-12}t^6 + 4.13 \times 10^{-9}t^5 - 6.32 \\ \varepsilon_r = -1.17 \times 10^{-15}t^7 - 1.59 \times 10^{-12}t^6 - 2.85 \times 10^{-9}t^5 + 2.94 \\ \varepsilon_t = \varepsilon_i + \varepsilon_r \end{cases} \quad (5b)$$

Fig. 10 shows the strain–time response of the incident and reflected pulses at high strain rates and the model curves predicted by the nonlinear regression equations. Fig. 10 also includes the actual measured transmissive strain signals from the SHPB test. Section 2.2.2, demonstrates that the sum of the incident and reflected strain signals is approximately equal to the transmissive signal in the test. Therefore, in this test, the actual measured transmitted strain signal was compared with the predicted incident and reflected signal curves to see if the predicted values matched the measured values as close as possible. The predicted strain signals were compared with the corresponding test values using a nonlinear fitting equation, and the predicted values were found to be a good predictor of the strain signals collected in the SHPB test.

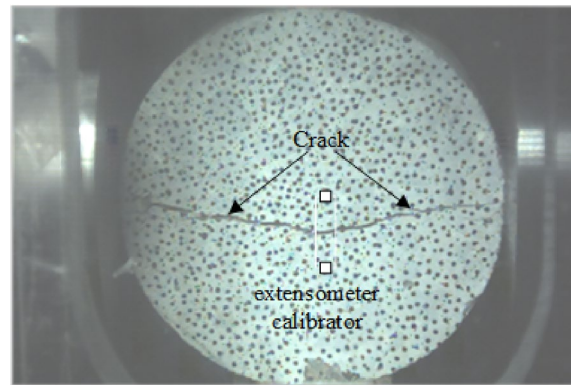
### 3.5 Failure Mode

The DIC technique is an image measurement technique based on numerical analysis, which can track the visible changes in the image and obtain the full-field displacement of the surface of the specimen by comparing the changes in the values of the scattered images before and after deformation. In this test, the displacement–strain field of high-strength concrete under a dynamic high-speed impact splitting test is analyzed based on the scatter images of specimens during damage acquired by high-speed cameras, and the crack development of

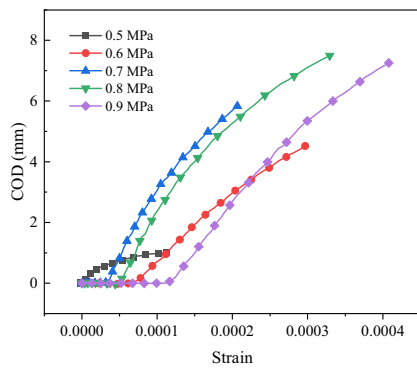
concrete specimens is detected and presented based on the DIC technique (Bhosale et al., 2020).

To further analyze the splitting process of high-strength concrete disc specimens at different impact strengths, the crack opening displacements (CODs) were used to track the crack development in this test. As shown in Fig. 11a, the position of the extensometer calibrator at the disc specimen is shown. For each extensometer calibrator, the crack opening displacements (CODs) can be evaluated by the difference between the displacements of two points in the Y-direction. Therefore, the COD–strain curves can be obtained at different impact pressures by the dynamic displacement field in the Y-direction calculated by DIC. The COD–strain curves of high-strength concrete discs under different impact pressures are shown in Fig. 11b, c. From Fig. 11b, it can be seen that in the C60 disc specimens, the crack opening displacements generally increase with the increase of impact pressure, and the COD values even reach 7 mm at impact pressures of 0.8 MPa and 0.9 MPa. Comparing Fig. 11b, c, it was found that the COD values of the C80 disc specimens are mostly higher than those of the C60 disc specimens. COD values are mostly smaller than those of C60, which is due to the higher strength of C80 concrete and, at the same time, its brittleness than that of C60.

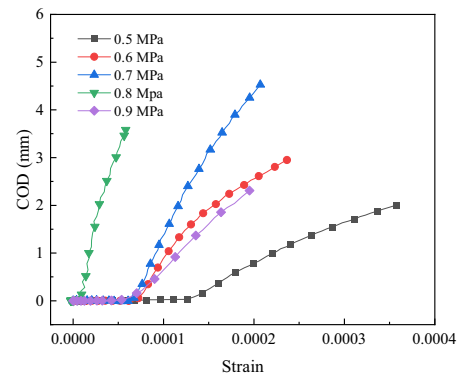
During the process of impact loading on concrete specimens, micro-strains and micro-cracks are accumulated inside the specimens and gradually develop into



(a) Location of the extensometer calibrator along the crack route

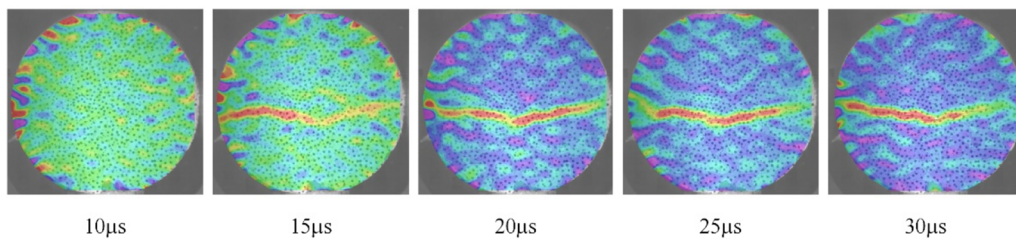


(b) C60 concrete specimens

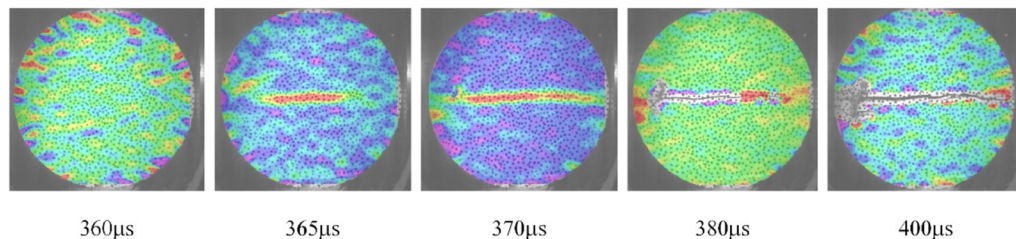


(c) C80 concrete specimens

**Fig. 11** DIC calculation results. **a** Location of the extensometer calibrator along the crack route. **b** The C60 COD–strain curve calculated by the DIC. **c** The C80 COD–strain curve calculated by the DIC.



(a) C60 concrete specimens



(b) C80 concrete specimens

**Fig. 12** Strain clouds of high-strength concrete under 0.05 MPa impact pressure.

micro-cracks and finally damage. As shown in Fig. 12, the DIC strain clouds of high-strength concrete (C60 and C80) under 0.05 MPa impact pressure are shown. It can be seen from the images that as the impact load increases, the micro-cracks carry out to reach the cementing surface and the stress reaches the peak point.

At this point, cracks appear on the surface of the specimens, and obvious red crack development traces appear in the images. With the continued loading of the impact load, the cracks continue to develop laterally until the specimens are completely damaged.

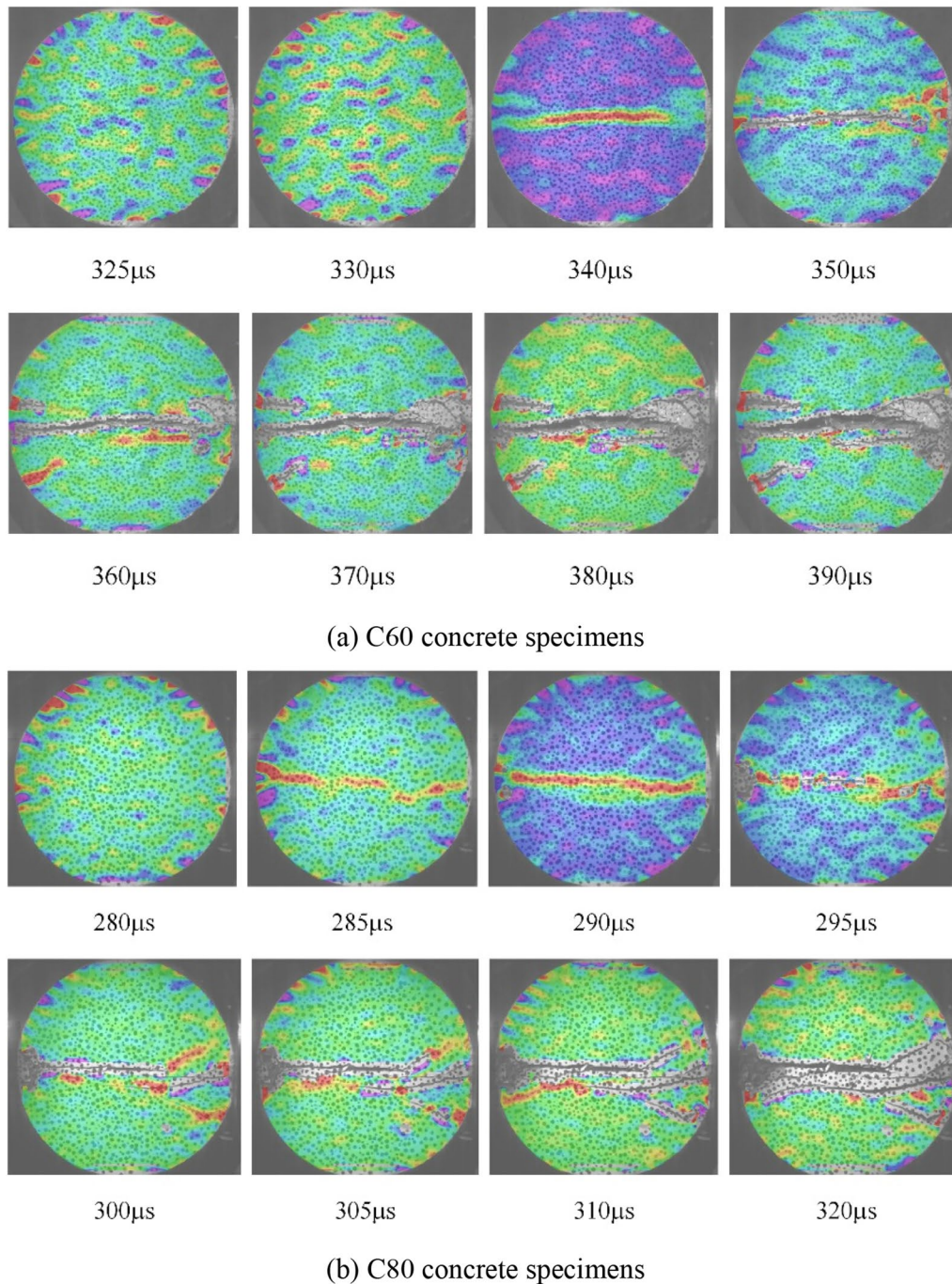


**Fig. 13** Strain cloud of high-strength concrete under 0.09 MPa impact pressure.

It is worth mentioning that by comparing Fig. 12a, b, it is found that the cracking time of C60 concrete specimens is earlier than that of C80 concrete specimens. At the same time, the crack expansion time until damage is about 25  $\mu\text{s}$  for C60 concrete specimens, while it is about 35  $\mu\text{s}$  for C80 concrete specimens. The time from macroscopic crack formation to specimens damage is shorter for C60 concrete specimens than for C80 specimens. This phenomenon corresponds to the results obtained in Sect. 3.2 of this study.

The critical damage strain for crack formation or development is one of the key issues in this study to enable the detection of damage patterns in concrete. In general, concrete is a quasi-brittle material with inherently weak tensile strength, when the strain values in concrete are relatively low. In this experiment, the crack paths in the potential damage zone of concrete were recorded and detected by the DIC technique, and then the damage zone of the specimens was mapped using the multiscale critical damage strain (Mamand et al., 2017; Bu et al., 2020), which includes both macroscopic and microscopic crack extensions. As shown in Fig. 13, the strain clouds of high-strength concrete specimens at high impact strength (at this point, high strain rate) are shown. As can be seen in Fig. 13a, the C60 specimens show a gradual concentration of stress between 325  $\mu\text{s}$  and 330  $\mu\text{s}$ . At 340  $\mu\text{s}$ , it can be observed that the stress concentration area expands from the middle of the specimens to both sides, and some micro-cracks start to develop gradually into macro cracks. In Fig. 13b, the time from the appearance of cracks to the complete damage destruction of the C80 specimens is 35  $\mu\text{s}$ , which is shorter than the time used for the C60 specimens (50  $\mu\text{s}$ ). Therefore, under a high strain rate, the concrete specimens with higher strength have a faster damage rate and, at the same time, higher crack extension.

Comparing the strain clouds of high-strength concrete specimens under different impact strengths in Figs. 12 and 13, it can be found that under the dynamic impact load, with the increase of impact strength, the strain rate also increases, and the instability of crack damage evolution pattern on the surface of high-strength concrete specimens increases. In addition, with the increase of impact load, the time from the appearance of cracks to the complete damage of high-strength concrete specimens grows, and the degree of cracking also increases. This phenomenon can prove that the brittleness of concrete increases with its strength, and at the same time, the brittle damage of concrete is more obvious with the increase in strain rate.

## 4 Conclusions

In this experiment, the splitting test properties of high-strength concrete were investigated based on the DIC technique. The SHPB test was used to investigate the splitting test damage form, stress–strain response, and dynamic dissipation energy of high-strength concrete at different impact strengths, and the time series prediction calculation model of the incident reflected and transmitted pulses of high-strength concrete specimens at high strain rates was established. The crack expansion during the splitting test of high-strength concrete at different impact strengths was also detected and analyzed based on the DIC technique, and the following conclusions were obtained.

- (1) The stress–strain curve of high-strength concrete is similar to that of ordinary concrete, with an initial approximate linear elastic phase, followed by a nonlinear phase increase of stress. After the stress reaches its peak, it enters the softening phase, in which the stress decreases less for high impact pressure.
- (2) The impact strength increased from 0.05 MPa to 0.09 MPa, and the peak strengths of C60 and C80 specimens increased by about 60% and 90%, respectively, and the dynamic splitting tensile strength of the specimens showed an overall trend of gradual increase in strain corresponding to the final damage.
- (3) The measured strain signals were fitted using a nonlinear fitting equation, and the predicted strain signals obtained were compared with the corresponding test values, and it was found that the predicted values using the one-dimensional nonlinear regression analysis equation could well predict the strain signals collected in the SHPB test.
- (4) Compared with the low impact pressure, the triangular damaged area at the end of the contact surface of the specimen and the rod subjected to high impact pressure increased significantly, the dynamic energy dissipation increased, and the damage degree of the specimen increased. The higher strength concrete specimens subjected to high strain rates had a faster damage rate, while the crack extension was also higher and the brittle damage was more pronounced.

The results of this study confirm that impact strength has a significant effect on the dynamic splitting test properties of high-strength concrete, determine the

crack initiation pattern during the dynamic splitting test process of high-strength concrete under different strain rates, and establish a strain–time fitting model for high-strength concrete at high strain rates. This provides a good experimental basis for further research on the dynamic splitting test properties of high-strength concrete and provides a theoretical basis for the design of high-strength concrete structures in practical engineering.

#### Abbreviations

SHPB: Separate Hopkinson pressure bar; DIC: Digital image correlation; COD: Crack opening displacement.

#### Acknowledgements

The authors would like to thank the financial support by National Key R&D Program of China (Grant No. 2021YFB2600200), National Natural Science Foundation of China (Grant No. 51979090) and State Key Laboratory of High-Performance Civil Engineering Materials (Grant NO. 2019CEM002).

#### Author contributions

XC: conceptualization and writing—original draft preparation. JW: conceptualization, formal analysis, writing—original draft preparation, and acquisition of data. KS: acquisition of data. YN: acquisition of data. LB: acquisition of data. All authors read and approved the final manuscript.

#### Authors' information

Xudong Chen: Professor, Ph. D, College of Civil and Transportation Engineering, Hohai University, Nanjing 210098, China.  
Jin Wu: Miss, Master's Student, College of Civil and Transportation Engineering, Hohai University, Nanjing 210098, China.  
Kai Shang: Mr, Bachelor, College of Civil and Transportation Engineering, Hohai University, Nanjing 210098, China.  
Yingjie Ning: Mr, Bachelor, Senior Engineer, Chief Engineer, Zhejiang Communications Construction Group Co., Ltd., Hangzhou 310051, China.  
Lihui Bai: Ms, Bachelor, Senior Engineer, Deputy Department Manager, Zhejiang Communications Construction Group Co., Ltd., Hangzhou 310051, China.

#### Funding

Not applicable.

#### Availability of data and materials

The data and materials are available.

#### Declarations

#### Ethics approval and consent to participate

Not applicable.

#### Consent for publication

All authors have read the final version of the manuscript and agree to its publication.

#### Competing interests

The authors declare that they have no competing interests.

#### Author details

<sup>1</sup>College of Civil and Transportation Engineering, Hohai University, Nanjing 210098, China. <sup>2</sup>Zhejiang Communications Construction Group Co., Ltd, Hangzhou 310051, China.

Received: 27 April 2022 Accepted: 4 July 2022

Published online: 05 August 2022

#### References

- Ai, D., Zhao, Y., Wang, Q., & Li, C. (2019). Experimental and numerical investigation of crack propagation and dynamic properties of rock in SHPB indirect tension test. *International Journal of Impact Engineering*, 126, 135–146.
- Bertholf, L. D., & Karnes, C. H. (1975). Two-dimensional analysis of the split Hopkinson pressure bar system. *Journal of the Mechanics and Physics of Solids*, 23(1), 1–19.
- Bhosale, A. B., & Prakash, S. S. (2020). Crack propagation analysis of synthetic vs. steel vs. hybrid fibre-reinforced concrete beams using digital image correlation technique. *International Journal of Concrete Structures and Materials*, 14(1), 1–19.
- Braunagel, M. J., & Griffith, W. A. (2020). A split Hopkinson pressure bar method for controlled rapid stress cycling using an oscillating double striker bar. *Rock Mechanics and Rock Engineering*, 53(8), 3845–3851.
- Bu, J., Chen, X., Hu, L., Yang, H., & Liu, S. (2020). Experimental study on crack propagation of concrete under various loading rates with digital image correlation method. *International Journal of Concrete Structures and Materials*, 14(1), 1–25.
- Chen, D., Liu, F., Yang, F., Jing, L., Feng, W., Lv, J., & Luo, Q. (2018). Dynamic compressive and splitting tensile response of unsaturated polyester polymer concrete material at different curing ages. *Construction and Building Materials*, 177, 477–498.
- Chen, H., Zhou, X., Li, Q., He, R., & Huang, X. (2021). Dynamic compressive strength tests of corroded SFRC exposed to drying-wetting cycles with a 37 mm diameter SHPB. *Materials*, 14(9), 2267.
- Chen, X., Ge, L., Zhou, J., & Wu, S. (2017). Dynamic Brazilian test of concrete using split Hopkinson pressure bar. *Materials and Structures*, 50(1), 1–15.
- Chen, X., Shi, D., & Guo, S. (2020). Experimental study on damage evaluation, pore structure and impact tensile behavior of 10-year-old concrete cores after exposure to high temperatures. *International Journal of Concrete Structures and Materials*, 14(1), 1–17.
- Chen, X., Wu, S., & Zhou, J. (2015). Compressive strength of concrete cores under high strain rates. *Journal of Performance of Constructed Facilities*, 29(1), 06014005.
- Dai, F., Huang, S., Xia, K., & Tan, Z. (2010). Some fundamental issues in dynamic compression and tension tests of rocks using split Hopkinson pressure bar. *Rock Mechanics and Rock Engineering*, 43(6), 657–666.
- Durand, B., Delvare, F., Bailly, P., & Picart, D. (2016). A split Hopkinson pressure bar device to carry out confined friction tests under high pressures. *International Journal of Impact Engineering*, 88, 54–60.
- Feng, W., Liu, F., Yang, F., Li, L., & Jing, L. (2018). Experimental study on dynamic split tensile properties of rubber concrete. *Construction and Building Materials*, 165, 675–687.
- Frew, D. J., Forrestal, M. J., & Chen, W. (2005). Pulse shaping techniques for testing elastic-plastic materials with a split Hopkinson pressure bar. *Experimental Mechanics*, 45(2), 186–195.
- Fu, Q., Zhao, X., Zhang, Z., Peng, G., Zeng, X., & Niu, D. (2021). Dynamic splitting tensile behaviour and statistical scaling law of hybrid basalt-polypropylene fibre-reinforced concrete. *Archives of Civil and Mechanical Engineering*, 21(4), 1–22.
- Gao, M. Z., Zhang, J. G., Li, S. W., Wang, M., Wang, Y. W., & Cui, P. F. (2020). Calculating changes in fractal dimension of surface cracks to quantify how the dynamic loading rate affects rock failure in deep mining. *Journal of Central South University*, 27(10), 3013–3024.
- GB, T50081–2002. (2002). Testing methods of mechanical properties of normal concrete. China: China Building Materials Academy.
- Gong, F. Q., Si, X. F., Li, X. B., & Wang, S. Y. (2019). Dynamic triaxial compression tests on sandstone at high strain rates and low confining pressures with split Hopkinson pressure bar. *International Journal of Rock Mechanics and Mining Sciences*, 113, 211–219.
- Hamrat, M., Boulekbache, B., Chemrouk, M., & Amziane, S. (2016). Flexural cracking behavior of normal strength, high strength and high strength fiber concrete beams, using Digital Image Correlation technique. *Construction and Building Materials*, 106, 678–692.
- Huang, B., & Xiao, Y. (2020). Compressive impact tests of lightweight concrete with 155-mm-diameter split hopkinson pressure bar. *Cement and Concrete Composites*, 114, 103816.
- Huang, R., Li, S., Meng, L., Jiang, D., & Li, P. (2020). Coupled effect of temperature and strain rate on mechanical properties of steel fiber-reinforced concrete. *International Journal of Concrete Structures and Materials*, 14(1), 1–15.

- Huang, Y., He, X., Wang, Q., & Xiao, J. (2019). Deformation field and crack analyses of concrete using digital image correlation method. *Frontiers of Structural and Civil Engineering*, 13(5), 1183–1199.
- Huang, Z., Chen, W., Hao, H., Aurelio, R., Li, Z., & Pham, T. M. (2022). Test of dynamic mechanical properties of ambient-cured geopolymer concrete using split Hopkinson pressure bar. *Journal of Materials in Civil Engineering*, 34(2), 04021440.
- Jiang, Z., Hu, C., Liu, M., Easa, S. M., & Zheng, X. (2020). Characteristics of morphology and tensile strength of asphalt mixtures under impact loading using split Hopkinson pressure bar. *Construction and Building Materials*, 260, 120443.
- Khan, M. Z. N., Hao, Y., & Hao, H. (2019). Mechanical properties and behaviour of high-strength plain and hybrid-fiber reinforced geopolymer composites under dynamic splitting tension. *Cement and Concrete Composites*, 104, 103343.
- Khosravani, M. R., & Weinberg, K. (2018). A review on split Hopkinson bar experiments on the dynamic characterisation of concrete. *Construction and Building Materials*, 190, 1264–1283.
- Li, C., Xu, Y., Chen, P., Li, H., & Lou, P. (2020). Dynamic mechanical properties and fragment fractal characteristics of fractured coal-rock-like combined bodies in split hopkinson pressure bar tests. *Natural Resources Research*, 29(5), 3179–3195.
- Li, M., Qian, C., & Sun, W. (2004). Mechanical properties of high-strength concrete after fire. *Cement and Concrete Research*, 34(6), 1001–1005.
- Li, X. B., Lok, T. S., Zhao, J., & Zhao, P. J. (2000). Oscillation elimination in the Hopkinson bar apparatus and resultant complete dynamic stress-strain curves for rocks. *International Journal of Rock Mechanics and Mining Sciences*, 37(7), 1055–1060.
- Liu, F., Ding, W., & Qiao, Y. (2019). Experimental investigation on the flexural behavior of hybrid steel-PVA fiber reinforced concrete containing fly ash and slag powder. *Construction and Building Materials*, 228, 116706.
- Mamand, H., & Chen, J. (2017). Extended digital image correlation method for mapping multiscale damage in concrete. *Journal of Materials in Civil Engineering*, 29(10), 04017179.
- Miao, Y. G. (2018). On loading ceramic-like materials using split Hopkinson pressure bar. *Acta Mechanica*, 229(8), 3437–3452.
- Mróz, K., Tekieli, M., & Hager, I. (2020). Feasibility study of digital image correlation in determining strains in concrete exposed to fire. *Materials*, 13(11), 2516.
- Pająk, M., Baranowski, P., Janiszewski, J., Kuciewicz, M., Mazurkiewicz, Ł., & Łażniewska-Piekarczyk, B. (2021). Experimental testing and 3D meso-scale numerical simulations of SCC subjected to high compression strain rates. *Construction and Building Materials*, 302, 124379.
- Pająk, M., Janiszewski, J., & Kruszka, L. (2019). Laboratory investigation on the influence of high compressive strain rates on the hybrid fibre reinforced self-compacting concrete. *Construction and Building Materials*, 227, 116687.
- Pan, B. (2018). Digital image correlation for surface deformation measurement: Historical developments, recent advances and future goals. *Measurement Science and Technology*, 29(8), 082001.
- Renliang, S., Yongwei, S., Liwei, S., & Yao, B. (2019). Dynamic property tests of frozen red sandstone using a split hopkinson pressure bar. *Earthquake Engineering and Engineering Vibration*, 18(3), 511–519.
- Ross, C. A., Tedesco, J. W., & Kuennen, S. T. (1995). Effects of strain rate on concrete strength. *Materials Journal*, 92(1), 37–47.
- Shah, S. G., & Chandra Kishen, J. M. (2011). Fracture properties of concrete-concrete interfaces using digital image correlation. *Experimental Mechanics*, 51(3), 303–313.
- Sharafisafa, M., Aliabadian, Z., & Shen, L. (2020). Crack initiation and failure development in bimrocks using digital image correlation under dynamic load. *Theoretical and Applied Fracture Mechanics*, 109, 102688.
- Sharafisafa, M., & Shen, L. (2020). Experimental investigation of dynamic fracture patterns of 3D printed rock-like material under impact with digital image correlation. *Rock Mechanics and Rock Engineering*, 53(8), 3589–3607.
- Skarżyński, Ł., & Suchorzewski, J. (2018). Mechanical and fracture properties of concrete reinforced with recycled and industrial steel fibers using Digital Image Correlation technique and X-ray micro computed tomography. *Construction and Building Materials*, 183, 283–299.
- Su, Y., Li, J., Wu, C., Wu, P., & Li, Z. X. (2016). Influences of nano-particles on dynamic strength of ultra-high performance concrete. *Composites Part B: Engineering*, 91, 595–609.
- Wu, B., Chen, R., & Xia, K. (2015). Dynamic tensile failure of rocks under static pre-tension. *International Journal of Rock Mechanics and Mining Sciences*, 80, 12–18.
- Yang, F., Ma, H., Jing, L., Zhao, L., & Wang, Z. (2015). Dynamic compressive and splitting tensile tests on mortar using split Hopkinson pressure bar technique. *Latin American Journal of Solids and Structures*, 12, 730–746.
- Zwiessler, R., Kenkmann, T., Poelchau, M. H., Nau, S., & Hess, S. (2017). On the use of a split Hopkinson pressure bar in structural geology: High strain rate deformation of Seeberger sandstone and Carrara marble under uniaxial compression. *Journal of Structural Geology*, 97, 225–236.

## Publisher's Note

Springer Nature remains neutral with regard to jurisdictional claims in published maps and institutional affiliations.

Submit your manuscript to a SpringerOpen<sup>®</sup> journal and benefit from:

- Convenient online submission
- Rigorous peer review
- Open access: articles freely available online
- High visibility within the field
- Retaining the copyright to your article

Submit your next manuscript at ► [springeropen.com](https://www.springeropen.com)